Desalination and Water Treatment
www.deswater.com
doi: 10.5004/dwt.2020.24895

177 (2020) 29–39
February

Simulation and performance analysis of reverse osmosis water desalination system operated by a high concentrated photovoltaic system

Adel A. Ghoneim*, Haitham A. Alabdulali

Applied Sciences Department, College of Technological Studies, Public Authority for Applied Education and Training (PAAET), P.O. Box: 42325, Shuwaikh 70654, Kuwait, emails: aa.ghoniem@paaet.edu.kw (A.A. Ghoneim), ha.alabdulali@paaet.edu.kw (H.A. Alabdulali)

Received 19 April 2019; Accepted 10 September 2019

ABSTRACT

This work examines the employment of high concentrated photovoltaic (HCPV) modules to drive reverse osmosis (RO) desalination unit in Kuwait weather. The RO systems which are operated by HCPV modules have several benefits, as low running expenses, easy running, simple setup and it is also environmentally friendly. An equivalent circuit model for single diode which is compatible with TRNSYS software is implemented to evaluate triple junction HCPV modules efficiency in Kuwait's environment considering concentration level and temperature effects. The performance of the RO unit powered by HCPV designed to provide drinking water at a constant daily load profile of 20 m^3/d to a community in a remote area in Kuwait is studied and optimized. A code consistent with available TRNSYS routines is developed to evaluate the efficiency of the RO unit in Kuwait's climate. The developed models are validated through comparison with experimental data available from literature. The efficiency of RO-HCPV unit is optimized by varying the different system parameters mainly: water salinity, water feed pressure, permeate water pressure, concentrate water pressure as well as permeate flow rate. In addition, HCPV modules slope and orientation are varied by running several simulations until the HCPV system size which satisfies the energy requirement needed is achieved. To explore the environmental effects of utilizing RO-HCPV system, the emissions of CO_2 avoided is calculated. The results show that an HCPV modules of inclination of 26° due south, which is about 0.88 of Kuwait latitude (29.5°), can attain maximum power generation. Current predictions reveal that a regular supply of 1.7 m^3/h leads to about 6,400 m^3 yearly from freshwater. Finally, the optimum HCPV modules slope which maximizes the reserved CO_2 emission corresponds to Kuwait' latitude and is equal to 2.1 ton/year.

Keywords: Solar desalination; High concentrated photovoltaic modules; Reverse osmosis; Solar radiation

1. Introduction

Available freshwater represents a very small percentage of the available water resources. Furthermore, about two-thirds of freshwater are commonly in snow and ice configuration on mountain areas and isolated islands. Population growth and evolved industrial development significantly increased the need for water sources and consequently results in water shortage. Suitable and efficient desalination of brackish water and seawater can certainly minimize current and anticipated future scarcity of water. The excessive need for conventional fuel resources is the primary disadvantage of the desalination process in addition to environmental pollution. Therefore, water desalination using renewable energy resources represents an interesting alternative in resolving water shortage. Renewable energy sources extensively exist in nature and at the same time, they are environmentally friendly. Many locations encounter water

* Corresponding author.

deficiency and at the same time have high irradiance as is the case in the Arabian Gulf regions. Making use of these interesting characteristics, renewable energy can economically be adapted to power different desalination methods to produce freshwater. Typically, electricity is utilized in membrane processes, whether for operating pumps with high pressure or salts ionization in seawater.

Reverse osmosis (RO) systems powered by photovoltaic (PV) solar modules are now regarded as a typical option in desalination plants [1–3] because PV and RO units' layouts are simple and basic [4]. Numerous researches are carried out involving the integration of PV and RO systems [5–7]. There are different types of solar systems in addition to various techniques that can be adapted to conduct the desalination process. Efficient setup methods are required for the desalination of seawater to consider the water quality, seawater salinity, environmental effects, energy efficiency and location variables [8,9]. Several standards must be considered when selecting an appropriate solar system such as working temperature, method of energy storage, type of solar system and system shape [10]. Integrating the two processes requires specific changes for reliable combination. Fortunately, most of solar desalination plants are combinations of components modified individually [11].

Herold and Neskakis [12] mounted an RO-PV system including storage batteries to store energy to generate 0.8–3 m^3/d of clean water. They concluded that when water pressure is 45 bar, the unit should be run for about 6 h to get the needed generation at energy usage of 16.3 kWh/m^3 and salinity of 450 ppm. Whilst utilizing a supply of 63 bar, enables the unit to obtain 0.16 m^3/h with 330 ppm salinity when using feed pressure of 63 bar and 15 kWh/m^3 of energy usage. Thomson and Infield [13] employed a MATLAB Simulink program to examine no storage RO-PV plant to generate 3 m^3/d of clean water. A PV array having single-axis tracking with 2.4 kW is used. Kumarasamy et al. [14] presented a code model to analyze an RO system powered by no battery PV array. Analytical optimization of the unit is carried out to calculate the optimum parameters for different situations, with no storage and with permeate storage.

Employing PV as an energy resource to drive the RO unit with a small size for freshwater generation is explored by Qiblawey et al. [15]. The proposed unit is assumed to be completely powered by PV arrays for situations with and without storage batteries. Sundaramoorthy et al. [16] presented a diffusion model proposing flow, pressure and solute concentration change in the membrane unit. A process proposing that membrane is nonporous media is presented by Kaghazchi et al. [17]. Abbas and Al-Bastaki [18] introduced the neural network's method to investigate an RO water desalination unit. Input model parameters are concentration, supply pressure, and temperature. The output parameter is the rate of permeate. Though, the presented model is only applied to units for which measurements are performed and cannot be applied for different RO systems.

A dynamical model for the RO system with permeates subsystem, brine subsystem and membrane subsystem is proposed by Gambier et al. [19]. Energy, mass and momentum conservation are employed to solve the equations of every subsystem. Though, the proposed method needs a lot of factors making its utilization a very complex one in the expert control system. Khayet et al. [20] modified an artificial neural network and response surface technique to analyze the RO-PV unit. Model inputs are feed flow, concentration, pressure, and temperature, where salt rejection and permeate flux are the model outputs. The energy requirement for the RO technique relies on the membrane characteristics as well as feed water salinity [21,22]. RO unit driven by PV arrays is more feasible and has more benefits to the environment than units operated by a diesel generator [23]. Off-grid RO-PV unit of capacity 72 gal/h at the Kingdom of Saudi Arabia can provide the freshwater needs for 250 people [24]. Hrayshat [25] simulations result for solar PV-RO units at ten places in Jordan revealed that feed water salinity and weather data have an important effect on freshwater production. Colangelo et al. [26] suggested numerical models for various shapes of RO units powered by a PV system. Al-Suleimani and Nair [27] discovered that a PV-RO system of 5 m^3/d having a life span of 25 years is more efficient than RO unit functioning with diesel and with the same capacity. The price of water generation per cubic meter was estimated to be 6.52 and 8.68 USD for a solar-powered RO and a diesel system, respectively.

Ullah and Rasul [28] presented an extensive review of the different desalination methods including the RO-PV system. RO-PV unit installed at Brisbane Botanic Garden, Australia is examined by Peterson and Gray [29]. The system generates about 3.36×10^6 L of permeate for 484 d for optimum water generation rate of 10,270 L/d during August 2009. A desalination unit powered by PV arrays for Abu Dhabi is examined by Kaya et al. [30]. The system analysis revealed that a PV unit with an efficiency of 20% can produce 511 kWh for each square meter at the price of $200. In addition, the RO-PV system can provide extra energy to the grid.

The cost of water production and the energy usage of the RO unit generally depend on the shape of the membrane and the ratio of total dissolved salts in water supply [31]. The expense of water generation and the usage of energy of the RO-PV combined units can be significantly decreased when employing PV modules with higher efficiency. Despite the great reduction in the prices of PV modules and land availability, higher initial expenses remain the major reasons for limiting the widespread of this system on a large scale. Nagaraj et al. [32] examined a hybrid energy system composed of solar PV, wind generator and battery to provide the required electricity for a desalination unit. They introduced an artificial neural network model to determine the total energy required for the proposed hybrid system. They concluded that the total annual energy evaluated employing the neural network technique is accurate and reliable.

In this current study, high concentrated photovoltaic (HCPV) modules are suggested to operate a small size RO water desalination unit. A single diode circuit model is developed to investigate the efficiency of HCPV modules considering the effects of both temperature and concentration factors. Additionally, a diode shunt resistance which is typically neglected in the established studies is accounted for in the model introduced for this work. To judge the precision and reliability of the present model, outcomes are compared to available experimental results. The current model results are in good agreement with corresponding measured data. To be able to simulate an RO system employing

TRNSYS software [33], a brand-new subroutine is developed compatible with different TRNSYS subroutines. The developed component is devoted to study and analyze the electric pump and the RO membranes. Location parameters as feed water properties, ambient temperature, and solar radiation are set as simulation inputs. The RO unit is suggested to generate 20 m^3/d of freshwater to fulfill the needs of people residing in a certain rural area in Kuwait. The recommended HCPV grid linked unit should be designed to generate the annual energy needed to operate the RO plant. Therefore, a constant supply of power is guaranteed to run the RO system without the necessity for extra expensive batteries. The influence of the HCPV area, HCPV tilt angle, water salinity and flow feed water on the freshwater production are analyzed. Lastly, the CO_2 emission avoided as a result of employing the HCPV system is assessed to inspect the environmental effects of the RO-HCPV system in Kuwait weather conditions. To our knowledge, this is the first work evaluating the efficiency of the HCPV-RO unit in Kuwait weather conditions.

2. Theoretical model of HCPV

Generally, there are various strategies and processes presented by researchers to calculate the efficiency of multi-junction PV cells as two diodes model for every sub-cell, single diode equivalent circuit model for each sub-cell, lumped diode model and network cell model. The numerical model adapted to evaluate the efficiency of HCPV cells should precisely take into account the variation of cell power vs. incident irradiance, ambient temperature as well as the concentration ratio of a solar cell. In the current work, a model for a single diode circuit of triple junctions PV cells is utilized to develop a numerical code to calculate the IV curve of the AZUR SPACE [34] triple-junction PV cell at various ambient temperatures, radiation intensities, and concentration ratio. The single diode model offers precise and dependable results and also it requires less empirical factors to be determined, that is, more time saving than the two diodes model which necessitates the determination of the empirical variables of multi-junction solar cell for every sub-cell. Fig. 1 is a schematic of a single diode equivalent circuit for multi-junction solar cells. The solar cell model consists of a current source which acts as a function of radiation in parallel with a diode. The present model can be extended for concentrator modules to account for potential differences resulted because of series resistance. Additionally, diode shunt resistance typically neglected in available models is considered in the present mathematical model.

Triple-junction cell composed of 3 junctions connected in series. Each connection described by single diode model. Current-voltage equation for every junction including shunt resistance is expressed as:

$$I_i = I_{\mathrm{sc},i} - I_{o,i}\left[e^{\frac{q\left(V_i+I_iR_{s,i}\right)}{n_ik_BT}}-1\right]-\frac{V_i+I_iR_{s,i}}{R_{\mathrm{sh},i}} \quad (1)$$

Each sub-cell utilizes 5 parameters: saturation current ($I_{o,i}$), short circuit current (I_{sc}), series and shunt resistances $R_{s,i}$ and $R_{\mathrm{sh},i}$ as well as ideality factor of the diode (n_i). T is cell temperature, V is voltages, k_B is Boltzmann constant, electron charge is q, I_i is load current; and express junction cell (1 for upper cell, 2 for medium cell and 3 for lower cell). Diode ideality factor (n) describes non-idealities in the diffusion diode. The main factor impacting the value of V_{oc}, is I_0 (reverse saturation current), which is a loss indicator for minority carriers through p-n junction in reverse bias. According to the theory of Shockley diodes ($n = 1$), however, values of n greater than unity is much suitable to consider defects generated during industrial procedures. R_s is the addition of the metal grids bulk resistance; bulk resistance of semiconductor materials and resistance of metal contact and the semiconductor. Series resistance, R_s, is regarded as the major factor helping to attain improved performance of the concentrated cells. Shunt resistance is a result of the leakage current through the p-n junction in the cell boundary or the crystal in the proximity to the junction because of imperfections or impurities deposition. V_{oc} is obtained by setting $I = 0$ in Eq. (1).

The last term in Eq. (1) leads to an implicit and nonlinear equation which requires great efforts to be solved. That is why this term is normally neglected in available models which presume that shunt resistance value is infinity. This assumption has a vital effect on the accuracy of the outcomes. Therefore, current work considers the shunt resistance. Utilizing Lambert W-function, Eq. (1) is varied from an implicit equation to an explicit nonlinear equation. Jain and

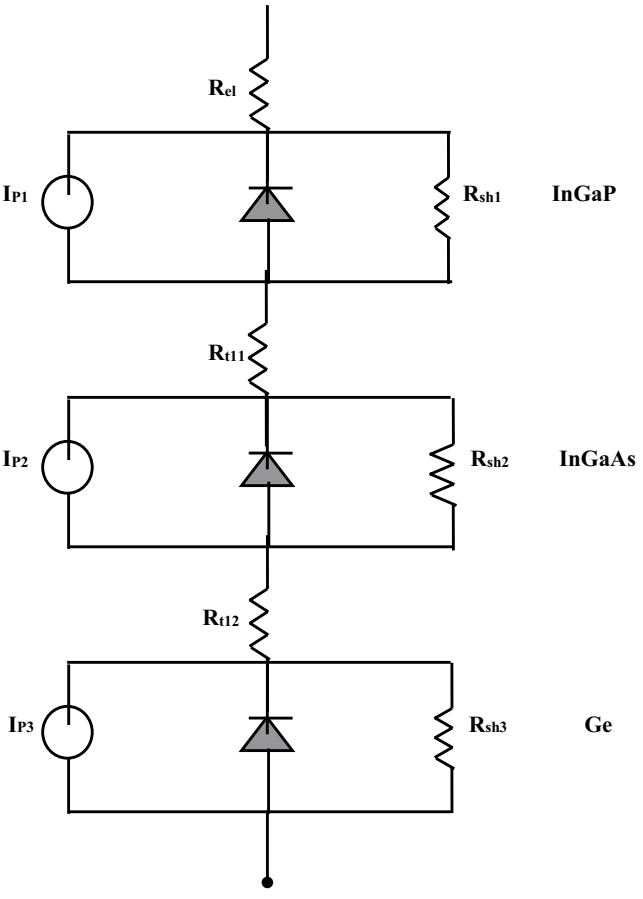

Fig. 1. Multi-junction HCPV cell single diode model.

Kapoor [35] adapted Lambert W-function to reformulate Eq. (1) as:

$$I_i = -\frac{V_i}{R_{s,i}+R_{\mathrm{sh},i}} - \frac{\text{Lambert W}\left\{\dfrac{R_{\mathrm{sh},i}\left(R_{s,i}I_{\mathrm{sc},i}+R_{s,i}I_{o,i}+V_i\right)}{\dfrac{nk_BT}{q}\left(R_{s,i}+R_{\mathrm{sh},i}\right)}\right\}\dfrac{nk_BT}{q}}{R_{s,i}} + \frac{R_{\mathrm{sh},i}\left(I_{o,i}+I_{\mathrm{sc},i}\right)}{R_{s,i}+R_{\mathrm{sh},i}} \quad (2)$$

Eq. (2) has an explicit characteristic that is why it is usually utilized to study PV systems [36,37]. Lambert W-function can be analyzed and resolved to employ already available mathematical software programs. The well-known Maple program is used to perform numerical model calculations. Ghoneim et al. [38] introduced a detailed numerical procedure to analyze and solve Eq. (2). The solar radiation absorbed by PV cells Q_{abs} is:

$$Q_{\mathrm{abs}} = X\,G\,A_{\mathrm{rec}}\eta_{\mathrm{op}} \quad (3)$$

where A_{rec} is the receiver area, G is the global radiation over the Fresnel lens in (W/m^2), η_{op} is the optical efficiency and X is the geometrical concentration factor of the HCPV optical system. The concentration factor (X) is the receiver area (A_{rec}) divided by the concentrator aperture area (A_{ap}). Triple-junction cells electrical efficiency (η_{el}) is correlated to both cell temperature T_{pvv} and concentration ratio X and is given by [39–42]:

$$\eta_{\mathrm{el}} = 0.298 + 0.0142\ln X + \left[-0.000715 + 0.0000697\ln X\right]\left(T_{\mathrm{pv}} - 298\right) \quad (4)$$

The optical, module and inverter efficiencies (η_{op},η_{mod}, η_{inv}) of the concentrator are assumed to be constant values, so the power generated is expressed as [39–42]:

$$P_{\mathrm{pv}} = XGA_{\mathrm{pv}}\eta_{\mathrm{op}}\eta_{\mathrm{mod}}\eta_{\mathrm{inv}}\eta_{\mathrm{el}} \quad (5)$$

where A_{pv} is the HCPV cells area.

Finally, to evaluate the electrical efficiency of the HCPV system, electrical efficiency (η_{el}) is determined by utilizing the equation [39–42]:

$$\eta_{\mathrm{el}} = \frac{P_{\mathrm{PV}}}{A_{\mathrm{ap}}G} = \frac{XGA_{\mathrm{PV}}\eta_{\mathrm{op}}\eta_{\mathrm{mod}}\eta_{\mathrm{inv}}\eta_{\mathrm{el}}}{A_{\mathrm{ap}}G} \quad (6)$$

Fill factor (FF) is given by:

$$\mathrm{FF} = \frac{P_m}{V_{\mathrm{oc}}I_{\mathrm{sc}}} = \frac{V_mI_m}{V_{\mathrm{oc}}I_{\mathrm{sc}}} \quad (7)$$

where V_m and I_m are maximum voltage and current at maximum power P_m.

The performance of a PV cell subjected to concentrated radiation will be enhanced. The short circuit current I_{sc} (Xsun) at concentration ratio X is expressed as:

$$I_{\mathrm{sc}}\left(X\mathrm{sun}\right) = XI_{\mathrm{sc}}\left(1\mathrm{sun}\right) \quad (8)$$

where I_{sc} (1sun) is short circuit current at 1sun (1,000W/m^2).

The introduced model is examined vs. available experimental data provided by the manufacturer of AZUR SPACE [34] high concentrated solar cells. The present predicted results agree well with the measurements recorded by the AZUR SPACE manufacturer.

3. RO design criteria and performance

The standard demand is to obtain the required freshwater over the whole day, so arrangements are necessary to consider the routine functioning of the system. The consumer must calibrate the flow rate to accommodate operation hours for every day. As an example, if 1,000 L per day freshwater is needed to be generated by an RO-HCPV unit and the unit works only 6 h daily, the chosen flow rate must be four times greater than the rate of flow for continuous daily operation. Characteristics of permeate flow rates together with supply water values are normally the inputs of simulation to select the proper pump and membrane. The following operating parameters need to be minimized as much as possible to precisely calculate the efficiency of the RO system: conductivity of permeate, the conductivity of supply, concentrate pressure, feed and permeate pressure, flow of permeate and temperature.

The operation procedure of the RO system is as follows: feed water gets into the RO membrane with high pressure adequate to get rid of osmotic pressure. Next, water molecules move through a semi-permeable membrane and salts and different contaminants are not allowed to pass and are sent through concentrate flow, which inputs to a drain or might be supplied once again to be reused across the RO system for water conservation. The energy demands for an RO process are mainly because of the pumping power, pretreatment process, and the high-pressure pumps. Energy required for the RO method is significantly reduced when employing two different techniques. The first technique is the improvement in the membrane manufacturing process to allow membranes to work effectively at low pressure and the second technique is using devices for energy restoration.

4. Numerical model of the RO process

Desalination consumes additional energy when compared to various types of water treatment and supply. Power required depends on different factors such as feed water temperature, water quality, system design, and employed technique. Furthermore, desalination methods of energy supply are a significant parameter as it is the major parameter influencing the price of freshwater. The energy required for desalination processes has been greatly reduced throughout the last few years due to the great enhancement in adapted processes and techniques which are anticipated to be further minimized shortly. Energy required for desalination methods can be minimized by controlling certain factors such as utilizing highly efficient pumps and employing advanced membrane materials.

To implement TRNSYS code to determine the efficiency of the RO unit, a novel subroutine compatible with other

TRNSYS subroutines is formulated and introduced. The developed subroutine is mainly dedicated to the simulation and analysis of the RO desalination unit and it consists of the high-pressure electric pump in addition to membranes. The membrane of the RO system is a fundamental component of the filtration process. Permeate water rate of flow (Q_P) is proportional to pressure difference through the membrane whilst the flow rate of salt is proportional to the change in concentration through the membrane and does not depend on the pressure applied. So, the flow rate of permeate across the membrane (Q_P) is a powerful correlation of the difference between osmotic pressure and supply pressure and is commonly expressed by the well-known formula:

$$Q_P = NA_m S_P \left(\Delta P - \Delta\pi\right) \tag{9}$$

where N is the membrane number, A_m is the area of the membrane and S_P is the permeability coefficient of the membrane. $\Delta\pi$ is the change between osmotic pressure on the supply side (π_f) and osmotic pressure of permeate (π_p), ΔP is the difference between average hydraulic pressure on the supply side (P_f) and hydraulic pressure of permeate (P_p). $\Delta\pi$ is a characteristic of the solution not related to the membrane, that is, it is a solution characteristic and does not depend on the membrane, and is usually expressed by the equation:

$$\Delta\pi = i\, C_i\, RT \tag{10}$$

where i is the number of ion species, C_i is molar concentration, R is ideal gas universal constant. Substituting Eq. (10) in Eq. (9) results in:

$$Q_P = NA_m S_{P:} \left(\Delta P - iC_i\, RT\right) \tag{11}$$

Considering the impact of the osmotic pressure of the permeate, permeate pressure, fouling factor and pressure variation in the RO vessel, Eq. (11) takes the form [43]:

$$Q_P = A_m S_P \left(\mathrm{TCF}\right)\left(\mathrm{FF}\right)\left[\left(P_{f-}\frac{\Delta P_{\mathrm{fc}}}{2} - P_p\right) - \left(\mathrm{CPF}\frac{\pi_f + \pi_b}{2} - \pi_P\right)\right] \tag{12}$$

The fouling factor (FF) is applied to the membrane to simulate aging and loss of permeability because of scale fouling. Normally, a fouling factor of 1 is assumed for a new membrane and a fouling factor between 0.65 to 0.85 for three-year-old membranes and older. P_p is the pressure of the permeate side which typically has the value of unity. In the RO process, increasing the temperature of feed water results in a rise in the permeate flow rate. So, one should adopt the correction parameter for temperature (TCF) and it is usually a correlation of the temperature of input water (T_w) in the form [43].

$$\mathrm{TCF} = \begin{Bmatrix} \exp\left[2{,}640\left(\frac{1}{198} - \frac{1}{273 + T_w}\right), T_w \geq 25^{\circ}\mathrm{C}\right] \\ \exp\left[3{,}020\left(\frac{1}{198} - \frac{1}{273 + T_w}\right), T_w < 25^{\circ}\mathrm{C}\right] \end{Bmatrix} \tag{13}$$

For a new membrane, TCF is equivalent to 1 and it decreases with increasing the filtration time of the RO unit. P_f is the feed water pressure getting into the membrane module. Pressure difference through the membrane module during the filtration procedure (ΔP_{fc}) can be expressed by the empirical formula [43]:

$$\Delta P_{\mathrm{fc}} = 0.756\left(\frac{Q_{\mathrm{c}} + Q_f}{2}\right)^{1.7} \tag{14}$$

Concentration factor of polarization, CPF, is expressed by the correlation [43]:

$$\mathrm{CPF} = e^{1.7Y} \tag{15}$$

where Y is the recovery ratio.

Utilizing previous formulas in Eq. (12), permeate flow rate and concentration can be evaluated. It should be noted that flow rates are assumed to be not compressible. Therefore, mass preservation can be adapted to calculate the total flow rate:

$$Q_f = Q_P + Q_C \tag{16}$$

All the above-mentioned RO membrane involved equations are formulated in a FORTRAN subroutine code compatible with other TRNSYS subroutines. To verify the precision and reliability of the current introduced RO model, the results of the current numerical model are calibrated vs. experimental data presented in the literature [44–46]. Present developed HCPV and RO models are verified separately as well as hybrid RO-HCPV by measured results. The comparison of different present models to experimental data indicated a mean average error of less than 4.5% in all models.

The RO component is then coupled with other TRNSYS subroutines to determine the performance of the proposed RO-HCPV system. The suggested RO-HCPV system comprises a membrane desalination system, HCPV modules, and an electric pump. The controller of the pump manages the power delivered to the membrane of the adapted desalination unit, which comprises a pump, membrane components, and other equipment. HCPV modules are connected directly to RO as presented in Fig. 2 as electrical power is needed to operate the high-pressure pump.

The unit consists of a set of batteries to store energy to maintain constant energy supply to the RO unit. In addition, a charge controller is employed to manage the batteries charge to eliminate overcharging. Batteries restrict the flow and pressure variations so that the system can produce freshwater of high quality. The different subroutines of system components are linked together and simulated using TRNSYS software.

5. Environmental impact of HCPV-RO system

Carbon dioxide (CO_2), methane (CH_4) and nitrous oxide (N_2O) are the most harmful gases from conventional sources of energy; but CO_2 is regarded as the principal parameter affecting worldwide global warming. That is why the

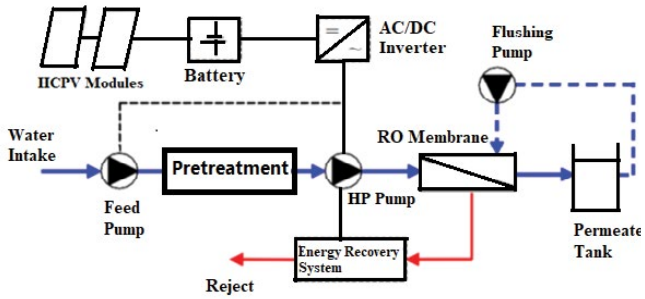

Fig. 2. Configuration of RO-HCPV system.

effects of CO_2 emissions only are studied in this work. The quantity of carbon emission eliminated through the utilization of renewable energy resources is related to both the type of conventional resource that is not utilized in addition to the conversion method employed to generate energy. Substituting a plant of larger CO_2 emission with a less emitting resource leads to a less CO_2 emission into the environment. This difference in CO_2 emitted is defined as the avoided CO_2 emission. The CO_2 emission decrease or CO_2 avoided emission is typically specified as the difference among emissions produced by traditional resources and emissions resulted during manufacturing the solar system through system lifetime which is usually 25 years. A mathematical code is developed to evaluate the avoided CO_2 emission accomplished when employing the RO-HCPV system instead of a conventional one. In this work, eliminated CO_2 emission (E_A) is primarily the emissions of CO_2 produced when utilizing traditional energy resources and is given by:

$$E_A = P_g \times F_E \tag{17}$$

where F_E is the emission factor of the plant (tonne CO_2/kWh) and P_g is the generated power (kWh).

To calculate CO_2 avoided emission because of the utilization of the HCPV system, it is necessary to specify the baseline electricity system. Frequently this will necessitate identifying a traditional system and the corresponding fuel type. Conversion efficiencies of various fuel types and the standard emission factors are the model input.

6. Results and discussions

Weather measurements used in this study are recorded by a set-up designed and installed at the College of Technological Studies, Kuwait (latitude 29.5°). Weather measurements contain typical values of hourly global radiation, ambient temperature and direct solar radiation for Kuwait during about 7 years in the time from 1st September 2011 until 15th January 2019. TRNSYS software is utilized to calculate the efficiency of the integrated system proposed. The time step of simulation in TRNSYS runs is adjusted to hourly simulation. Fig. 3 presents the change of the examined HCPV cell efficiency (h) with a concentration ratio for various temperatures with the data measured by the AZUR SPACE cell manufacturer. The efficiency behavior is the same as V_{oc} behavior and it is in excellent agreement with previous results introduced by Nishioka et al. [47]. Root

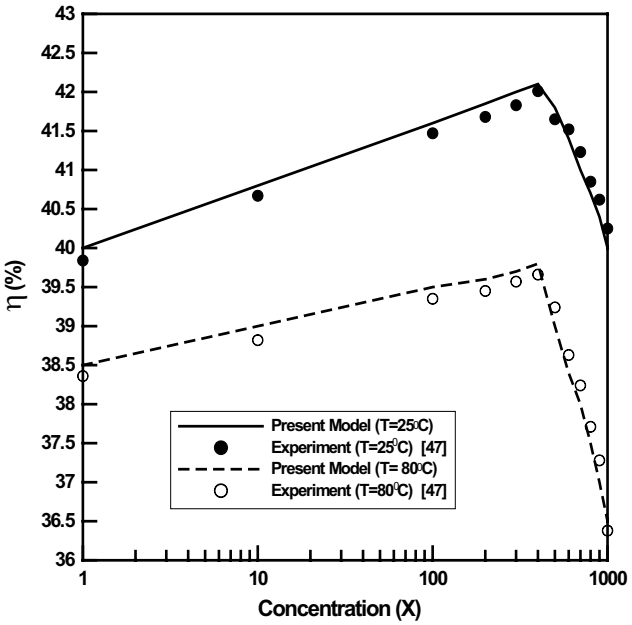

Fig. 3. Change of HCPV efficiency against concentration ratio for AZUR SPACE cells.

mean square (RMS) error in HCPV electrical efficiency calculations is about 1.2%.

As illustrated by Fig. 3, η rises against concentration until the concentration level reaches about 400 suns. This rise is restrained by logarithmic growth in V_{oc} as radiation increases. Though, when concentration rises, the behavior is adjusted by fill factor decrease due to series resistance losses. Accordingly, efficiency reduces in certain concentration levels. In addition, the temperature dependency of efficiency decreases with concentration. The above-mentioned outcomes illustrate that current results for multi-junction AZUR SPACE cells agree well with similar experimental data. This lets us state that current predictions accurately determine the performance of HCPV modules through a wide range of working parameters.

In the beginning, the size of the HCPV modules is calculated considering overall loads of the RO unit. To assure the oversizing of the HCPV-RO system and that it runs efficiently, two factors are considered RO-load size which is pump size, and seasonal irradiance variations. The number of HCPV arrays required to produce the required power is determined by the HCPV system needed to power the RO system. Stand-alone (off-grid) HCPV system sizing necessitates calculating the RO system energy consumption as well as incident radiation. To accomplish the design needed, the HCPV cell's maximum power is estimated at standard test conditions (air mass = 1.5, global radiation = 1,000 W/m^2 and ambient temperature 25°C).

Standalone HCPV system size and performance have been studied by the TRNSYS program. TRNSYS software is employed to determine the behavior of HCPV cells throughout the day when solar radiation is available. Required energy provided by HCPV modules and battery storage is utilized to power the RO unit when solar intensity is low. Energy produced from HCPV modules changes due to the

variations in insolation and ambient temperature. The mean daily energy produced is evaluated for different months.

The flow rate of the permeate greatly depends on PV output power, that is, it depends on the modules overall area. So, it is crucial to examine the effect of HCPV output power on permeate flow. Therefore, feedwater flow is held fixed at 40 m^3/d with salinity of 12,000 mg/L. The simulated and measured [45] permeate flow rate vs. HCPV output power is presented in Fig. 4. Graphs are fitted for simulation and measurement results to investigate data behavior. Equations of both predictions are found to be polynomial of third-degree indicating that neither measured nor theoretical predictions are a linear function of HCPV power. As shown by the figure, simulated predictions are in good agreement with measured data with a mean percent error of 4.18%, which validates the reliability of the present developed model.

The flow rate of permeate Q_P is directly proportional to the pumping power, that is, it is proportional to operating pressure difference through the membrane. HCPV power is supplied to the RO system to run a high-pressure pump. It is also found that approximately 42 kWh HCPV-peak power is required for a daily generation of 20 m^3 freshwater for the studied remote area in Kuwait, that is, about 2.1 kWh/m^3.

The slope of HCPV modules is a crucial parameter that influences permeate flow rate as the tilt variation affects radiations reaching the surface of HCPV modules. Changes in permeate flow rate for different modules inclination for various seasons are examined. The slope of the module is changed from zero up to 90 using a 5° step. The slope of HCPV is noticed to have an important influence on the flow rate of permeate particularly in summer season compared to winter outcomes. The zenith angle is also varied from zero at solar noon to 90° at sunrise and then steadily increases to 90° (at sunset) in summer but it is decreased to 45° in winter and then regularly rises to 90° at sunset. Winter permeate flow rate is 8 m^3/d for horizontal HCPV modules, and it grows to 12 m^3/d for 35° tilt. An additional rise in the inclination reduces the flow rate of permeate. So, modules with tilt values between 35° and 45° are more important from the permeate flow rate. This behavior is mainly because at noon, the angle of zenith is 45°, and since HCPV tilt is constant up to this magnitude then it accumulates maximum radiation resulting in extra HCPV energy which generates more permeate flow rate. The maximum flow rate of permeate in summer changes from 23 to 5 m^3/d if the slope of the HCPV module is changed from 0 to 90°. The maximum permeate flow rate is attained for HCPV modules with zero slopes because of the concept that the angle of zenith is nearly zero at noon, so horizontal HCPV modules achieve optimum solar radiation at this time causing an increase in generated HCPV power and accordingly increasing the permeate flow rate. For various HCPV slopes, solar radiations gained by HCPV panels are smaller producing less permeate flow rate.

Because of the high expenses and other technical complexes of the tracking system, it is more suitable to evaluate the yearly optimum HCPV tilt. Fig. 5 shows the rate of freshwater per year for HCPV modules with a tilt angle varying from 0° to 90° with modules facing south (zero azimuth angle). The calculated permeate is 1,850 m^3 per year for flat HCPV modules and 890 m^3 for 90° HCPV orientation. It is found that the maximum permeates collected per year is 6,400 m^3 which is attained when the HCPV slope angle is 26°. This prediction agrees well with Chang [48] result who stated that the optimum slope for south-facing HCPV modules for latitudes less than 65° is about 90% of the location latitude. The optimal yearly slope angle based on current predictions is 26° and it equals about 88% of Kuwait's latitude (29.5°).

The RO-desalination unit is supposed to supply 20 m^3/d of freshwater and the recovery percentage of the RO unit that will be utilized is 50%. Therefore, the daily brackish

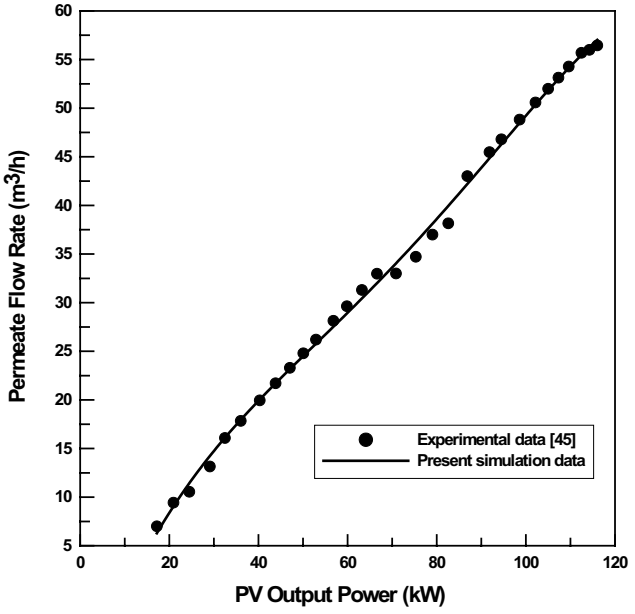

Fig. 4. Simulated and measured data of permeate water at different HCPV power.

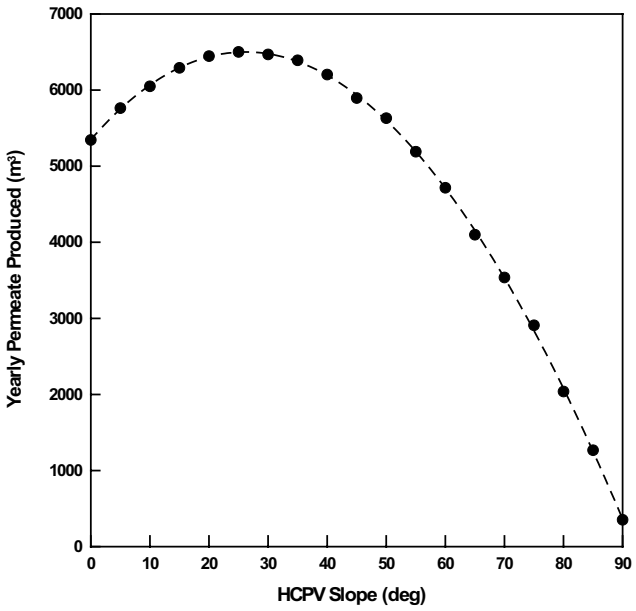

Fig. 5. Yearly permeate water for different HCPV module inclination.

water required will be 40 m^3. It is found that permeate water production (Q_p) is greatly a linear function of Kuwait solar radiation. Fig. 6 presents the permeate water produced for each month of the year along with the required freshwater for HCPV modules optimum tilt angle. As illustrated in Fig. 6, production of pure water in summer months satisfies the area needs from freshwater. This means that the RO unit operated by the HCPV system can satisfy the area needs from freshwater during the summer months. At the same time, the unit can supply a reasonable part of freshwater needs in winter months. The simulation results show that the desalination plant will produce fresh desalinated water of about 6,400 m^3 yearly utilizing regular brackish feed water of 40 m^3/d correspondings to a daily average of about 17 m^3/d. Good running membrane filtration system has stable radiation and low energy consumption. To attain these aims, the procedure should be optimized regarding permeate product, pressure, and temperature.

The salinity of feedwater flow has a significant impact on the flow of fresh water produced. Rising the feedwater salinity results in a decrease in the flow of clean water as illustrated in Fig. 7 because of the rise in osmotic pressure. So, in this situation, it is interesting to improve the number or permeability of membranes. This means that the system designer must search for a membrane-type compatible with the characteristics of the feed water.

The precise calculation of CO_2 avoided emissions due to utilizing HCPV modules, must consider CO_2 emission produced during the manufacturing of HCPV different components. Generally, the rate of CO_2 emissions from HCPV modules is much lower than the CO_2 emission rate produced from traditional energy resources, therefore it is ignored in this work. Annual avoided CO_2 emission change vs. HCPV modules slope is illustrated in Fig. 8.

Fig. 8 implies that the CO_2 emission eliminated is maximum at an optimum slope angle of 29° which is very near to the latitude of Kuwait (29.5°). The emissions of CO_2 avoided at this angle is about 2.1 ton/year. These predictions verify the environmental effects of the grid-tied RO-HCPV unit in Kuwait weather conditions. Furthermore, the expenses expected when implementing the Kyoto Protocol, that applying penalties in the case of emissions of the greenhouse effect must be included in the prices of fossil fuel sources. Though Kyoto Protocol is not at present applied in Kuwait, nevertheless regarding the use of this protocol will promote the cost-effective and environmental impacts of RO-HCPV systems substantially. Lastly, it is important to state that the feasibility of RO-HCPV is not examined in the present work. However, it is essential to complete this work by analyzing the economic aspects of RO-HCPV systems in Kuwait. This knowledge will advise the government in examining the power of grid-connected solar energy systems in Kuwaiti weather conditions.

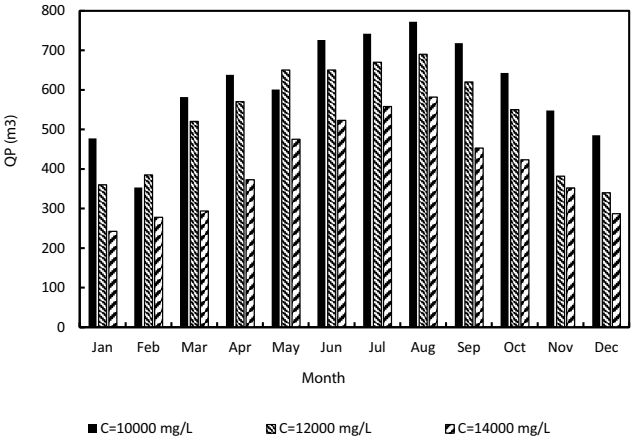

Fig. 7. Impact of feed water salinity on freshwater production.

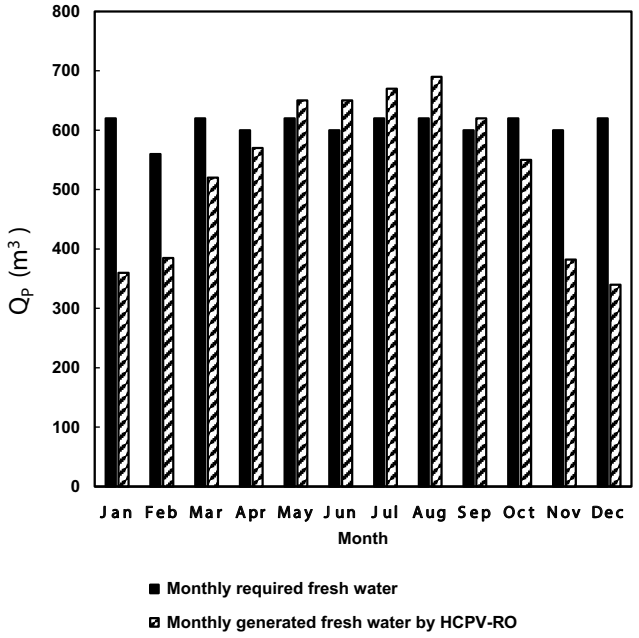

Fig. 6. Monthly freshwater production.

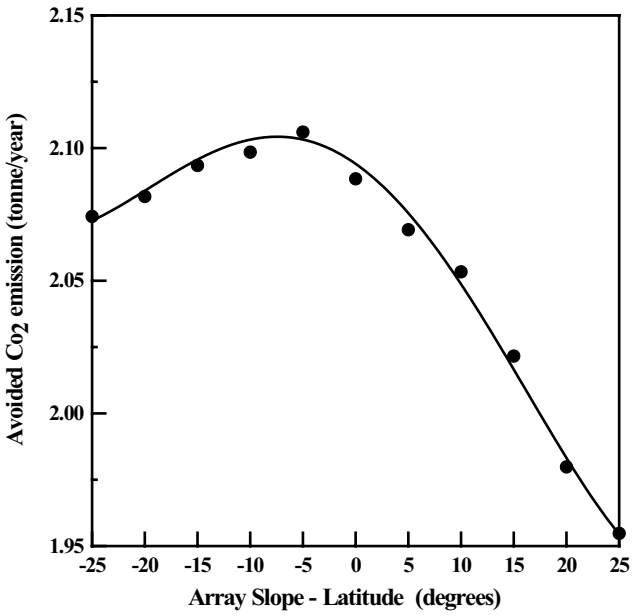

Fig. 8. Annual avoided CO_2 emission vs. HCPV slope angle.

7. Conclusions

In the present work, theoretical techniques are successfully developed to examine the performance of the RO-HCPV desalination unit. A new TRNSYS subroutine compatible with other components is developed and linked to other standard TRNSYS components to carry out the present simulation analysis. The equivalent circuit model for a single diode that is compatible with TRNSYS software is adapted to determine HCPV efficiency in Kuwait's environment considering concentration level and temperature effects. The RO unit powered by HCPV is designed to provide drinking water at the rate of 20 m^3/d to a community in a remote area in Kuwait. A subroutine appropriate for TRNSYS software is developed to examine RO performance in Kuwait's climate. The developed RO-HCPV model is calibrated against measurement data in literature. Depending on the present predictions, the following concluding statements are revealed:

- The model of a single diode is an acceptable model for effective purposes instead of utilizing the sophisticated two diodes model. Current results have an overall RMS error of less than 2% in comparison with published measured data.
- RMS error in the efficiency of HCPV modules is about 1.2%.
- Simulated data for the RO-HCPV system agree well with the corresponding experimental data with a mean percent error of 4.18% which validates the reliability of the present developed model.
- Prediction of simulations indicates that the freshwater generation changes linearly vs. solar radiation.
- A daily production of 20 m^3 of fresh water for the studied remote area in Kuwait requires HCPV modules of peak power 42 kWh, that is, about 2.1 kWh/m^3 is needed.
- HCPV module slope angle has an important influence on the produced fresh water. Maximum permeate production corresponds to the yearly optimal HCPV tilt angle of 26° which corresponds to about 0.88 times the latitude of Kuwait (29.5°).
- RO unit powered by the HCPV system can satisfy the area needs from freshwater in summer months while it can supply a reasonable part of freshwater needs in winter months.
- Utilizing brackish feed water of 40 m^3/d, RO-HCPV desalination plant can produce freshwater of about 6,400 m^3/year corresponding to a daily average production of about 17 m^3/d.
- Increasing feed water salinity results in a decrease in freshwater flow because of the increase in osmotic pressure.
- The optimum HCPV tilt angle which maximizes the CO_2 emission avoided is almost equal to Kuwait's latitude (29.5)°. At this optimum tilt angle, the CO_2 emission eliminated equals approximately 2.1 ton/year.
- The present results confirm the environmental impacts of the integrated RO-HCPV unit in Kuwait's climate.
- It is important to complete this study by carrying out a feasibility study to determine the life cycle cost of the RO-HCPV unit. This will necessitate the precise evaluation of each component cost as well as other installations and maintenance costs.

Acknowledgments

This research was financed by the Public Authority for Applied Education and Training (PAAET), Kuwait Project No. TS-18-02. The research team would like to express their utmost gratitude and appreciation to the Public Authority for Applied Education and Training (PAAET) at Kuwait for their generous financial support and assistance without which the completion of this research would not have been possible.

Symbols

A_{ap}	—	Concentrator aperture area, m^2
A_m	—	Membrane area, m^2
A_{rec}	—	Receiver area, m^2
A_{pv}	—	HCPV cells area, m^2
CPF	—	Concentration factor of polarization, -
C_i	—	Molar concentration, mol/m^3
E_A	—	Eliminated CO_2 emission, ton
F_E	—	Plant emission factor, ton/kWh
FF	—	Fouling factor, -
G	—	Global solar radiation on collector surface, W/m^2
I_i	—	Load current, A
I_m	—	Maximum current, A
I_o	—	Saturation current, A
I_{sc}	—	Short circuit current, A
k_B	—	Boltzmann constant, J/K
n	—	Ideality factor of the diode, -
N	—	Membrane number, -
P_f	—	Pressure on supply side, N/m^2
P_m	—	Maximum power, W
P_p	—	Hydraulic pressure of permeate, N/m^2
q	—	Electron charge, C
Q_{abs}	—	Solar radiation absorbed by PV cells, W
Q_C	—	Concentrate flow rate, m^3
Q_f	—	Total flow rate, m^3
Q_P	—	Rate of permeate across membrane, m^3
R	—	Gas universal constant, J/mol K
R_s	—	Series resistance, W
R_{sh}	—	Shunt resistance, W
S_p	—	Permeability coefficient of membrane, -
T	—	Temperature, K
T_w	—	Input water temperature, K
T_{pv}	—	Cell temperature, K
V	—	Voltage, V
V_{oc}	—	Open circuit voltage, V
V_m	—	Maximum voltage, V
X	—	Concentration factor, -
Y	—	Recovery ratio, -
η_{el}	—	Solar cells electrical efficiency, -
η_{inv}	—	Inverter efficiencies, -
η_{mod}	—	Module efficiencies, -
η_{op}	—	Optical efficiency, -
π_f	—	Osmotic pressure on supply side, N/m^2
π_p	—	Osmotic pressure of permeate, N/m^2
ΔP_{fc}	—	Pressure difference through membrane during filtration, N/m^2
$\Delta\pi$	—	Osmotic pressure change, N/m^2

References

[1] S.M. Hasnain, S.A. Alajlan, Coupling of PV-powered R.O. brackish water desalination plant with solar stills, Desalination, 116 (1998) 57–64.

[2] S. Alawaji, M.S. Smiai, S. Rafique, B. Stafford, PV-powered water pumping and desalination plant for remote areas in Saudi Arabia, Appl. Energy,52 (1995) 283–289.

[3] S.A. Alajlan, M.S. Smiai, Performance and development of PV - plant for water pumping and desalination for remote area in Saudi Arabia, Renewable Energy, 8 (1996) 441–446.

[4] B. Parida, S. Iniyan, R.R. Goic, A review of solar photovoltaic technologies, Renewable Sustainable Energy Rev.,15 (2011) 1625–1636.

[5] E.Sh. Mohamed, G. Papadakis, E. Mathioulakis, V. Belessiotis, A direct coupled photovoltaic seawater reverse osmosis desalination system toward battery based systems — a technical and economical experimental comparative study, Desalination, 221 (2008) 17–22.

[6] V. Amati, C.H. Zapater, E. Sciubba, J.U. Marcuello, Process Simulation of a Reverse Osmosis Desalination Plant Powered by Photovoltaic Panels for Kalymnos Island, ASME 2008 International Mechanical Engineering Congress and Exposition, Boston, Massachusetts, USA, 2008, pp. 209–217.

[7] E.Sh. Mohamed, G. Papadakis, Design, simulation and economic analysis of a stand-alone reverse osmosis desalination unit powered by wind turbines and photovoltaics, Desalination, 164 (2004) 87–97.

[8] P.E. Minton, Handbook of Evaporation Technology, Noyes Publications, 1986.

[9] A. Gastli, Y. Charabi, S. Zekri, GIS-based assessment of combined CSP electric power and seawater desalination plant for Duqum—Oman, Renewable Sustainable Energy Rev., 14 (2010) 821–827.

[10] O.A. Hamed, E.I. Eisa, W.E. Abdalla, Overview of solar desalination, Desalination, 93 (1993) 563–579.

[11] M. Papapetrou, M. Wieghaus, C. Biercamp, Roadmap for the Development of Desalination Powered by Renewable Energy – Promotion of Renewable Energy for Water Production Through Desalination, Fraunhofer ISE, Freiburg im Breisgau, 2010.

[12] D. Herold, A. Neskakis, A small PV-driven reverse osmosis desalination plant on the island of Gran Canaria, Desalination, 137 (2001) 285–292.

[13] M. Thomson, D. Infield, A photovoltaic-powered seawater reverse-osmosis system without batteries, Desalination, 153 (2002) 1–8.

[14] S. Kumarasamy, S. Narasimhan, S. Narasimhan, Optimal operation of battery-less solar powered reverse osmosis plant for desalination, Desalination, 375 (2015) 89–99.

[15] H. Qiblawey, F. Banat, Q. Al-Nasser, Performance of reverse osmosis pilot plant powered by photovoltaic in Jordan, Renewable Energy, 36 (2011) 3452–3460.

[16] S. Sundaramoorthy, G. Srinivasan, D.V.R. Murthy, An analytical model for spiral wound reverse osmosis membrane modules: Part I — model development and parameter estimation, Desalination, 280 (2011) 1403–1411.

[17] T. Kaghazchi, M. Mehri, M.T. Ravanchi, A. Kargari, A mathematical modeling of two industrial seawater desalination plants in the Persian Gulf region, Desalination, 252 (2010) 135–142.

[18] A. Abbas, N. Al-Bastaki, Modeling of an RO water desalination unit using neural networks, Chem. Eng. J., 114 (2005) 139–143.

[19] A. Gambier, A. Krasnik, E. Badreddin, Dynamic Modeling of a Simple Reverse Osmosis Desalination Plant for Advanced Control Purposes, Proceedings of the 2007 American Control Conference, IEEE, Marriott Marquis Hotel at Times Square New York City, USA, July 11e13, 2007.

[20] M. Khayet, C. Cojocaru, M. Essalhi, Artificial neural network modeling and response surface methodology of desalination by reverse osmosis, J. Membr. Sci., 368 (2011) 202–214.

[21] L.F. Greenlee, D.F. Lawler, B.D. Freeman, B. Marrot, P. Moulin, Reverse osmosis desalination: water sources, technology, and today's challenges, Water Res.,43 (2009) 2317–2348.

[22] S. Abdallah, M. Abu-Hilal, M.S. Mohsen, Performance of a photovoltaic powered reverse osmosis system under local climatic conditions, Desalination,183 (2005) 95–104.

[23] W. Gocht, A. Sommerfeld, R. Rautenbach, Th. Melin, L. Eilers, A. Neskakis, D. Herold, V. Horstmann, M. Kabariti, A. Muhaidat, Decentralized desalination of brackish water by a directly coupled reverse-osmosis-photovoltaic-system - a pilot plant study in Jordan, Renewable Energy,14 (1998) 287–292.

[24] W.W. Boesch, World's first solar powered reverse osmosis desalination plant, Desalination, 41 (1982) 233–237.

[25] E.S. Hrayshat, Brackish water desalination by a stand alone reverse osmosis desalination unit powered by photovoltaic solar energy, Renewable Energy, 33 (2008) 1784–1790.

[26] A. Colangelo, D. Marano, G. Spagna, V.K. Sharma, Photovoltaic powered reverse osmosis sea-water desalination systems, Appl. Energy, 64 (1999) 289–305.

[27] Z. Al-Suleimani, V.R. Nair, Desalination by solar-powered reverse osmosis in a remote area of the Sultanate of Oman, Appl. Energy, 65 (2000) 367–380.

[28] I. Ullah, M.G. Rasul, Recent developments in solar thermal desalination technologies: a review, Energies, 12 (2019) 119.

[29] E.L. Peterson, S.R. Gray, Effectiveness of desalination powered by a tracking solar array to treat saline bore water, Desalination, 293 (2012) 94–103.

[30] A. Kaya, M.E. Tok, M. Koc, A levelized cost analysis for solar-energy-powered sea water desalination in the Emirate of Abu Dhabi, Sustainability, 11 (2019) 1691.

[31] H.M. Laborde, K.B. França, H. Neff, A.M.N. Lima, Optimization strategy for a small-scale reverse osmosis water desalination system based on solar energy, Desalination, 133 (2001) 1–12.

[32] R. Nagaraj, D.T. Murthy, M.M. Rajput, Modeling renewables based hybrid power system with desalination plant load using neural networks, Distrib. Gener. Altern. Energy J., 34 (2019) 32–46.

[33] S.A. Klein, W.A. Beckman, J.W. Mitchell, J.A. Duffie, N.A. Duffie, T.L. Freeman, J.C. Mitchell, J.E. Braun, B.L. Evans, J.P. Kummer, R.E. Urban, A. Fiksel, J.W. Thornton, N.J. Blair, P.M. Williams, D.E. Bradley, T.P. McDowell, M. Kummert, D.A. Arias, TRNSYS, A Transient System Simulation Program Manual, Solar Energy Laboratory, University of Wisconsin – Madison, USA, 2016.

[34] Azurspace Solar Power GmbH, 2018. Available at: www.azurspace.com.

[35] A. Jain, A. Kapoor, Exact analytical solutions of the parameters of real solar cells using Lambert W-function, Sol. Energy Mater. Sol. Cells, 81 (2004) 269–277.

[36] F. Ghani, M. Duke, Numerical determination of parasitic resistances of a solar cell using the Lambert W-function, Sol. Energy, 85 (2011) 2386–2394.

[37] F. Ghani, G. Rosengarten, M. Duke, J.K. Carson, On the influence of temperature on crystalline silicon solar cell characterization parameters, Sol. Energy, 112 (2015) 437–445.

[38] A.A. Ghoneim, K.M. Kandil, T.H. Alzanki, M.R. Alenezi, Performance analysis of high-concentrated multi-junction solar cells in hot climate, Int. J. Sustainable Energy, 37 (2018) 294–310.

[39] A. Kribus, K. Daniel, G. Mittelman, A. Hirshfeld, Y. Flitsanov, A. Dayan, A miniature concentrating photovoltaic and thermal system, Energy Convers. Manage., 47 (2006) 3582–3591.

[40] M. Li, X. Ji, G. Li, S. Wei, Y.F. Li, F. Shi, Performance study of solar cell arrays based on a trough concentrating photovoltaic/thermal system, Appl. Energy, 88 (2011) 3218–3227.

[41] F. Calise, L. Vanoli, Parabolic trough photovoltaic/thermal collectors: design and simulation model, Energies, 5 (2012) 4186–4208.

[42] A. Buonomano, F. Calise, M.D. d'Accadia, L.A. Vanoli, A novel solar trigeneration system based on concentrating photovoltaic/thermal collectors. Part 1: design and simulation model, Energy, 61 (2013) 59–71.

[43] DOW Filmtec™ Membranes, Filmtec™ Reverse Osmosis Membranes: Technical Manual, Form No. 609–00071–0705, 2018. Available at: http://www.dowwaterandprocess.com/en.

[44] L. Song, K.G. Tay, Performance prediction of a long crossflow reverse osmosis membrane channel, J. Membr. Sci., 281 (2006) 163–169.

[45] E.M. Van Wagner, A.C. Sagle, M.M. Sharma, B.D. Freeman, Effect of crossflow testing conditions, including feed pH and continuous feed filtration, on commercial reverse osmosis membrane performance, J. Membr. Sci., 345 (2009) 97–109.
[46] S. Sundaramoorthy, G. Srinivasan, D.V.R. Murthy, An analytical model for spiral wound reverse osmosis membrane modules: Part II — experimental validation, Desalination, 277 (2011) 257–264.
[47] K. Nishioka, T. Takamoto, T. Agui, T. Kaneiwa, Y. Uraoka, Y.T. Fuyuki, Evaluation of temperature characteristics of high-efficiency InGaP/InGaAs/Ge triple-junction solar cells under concentration, Sol. Energy Mater. Sol. Cells, 85 (2015) 429–436.
[48] T.P. Chang, Output energy of a photovoltaic module mounted on a single-axis tracking system, Appl. Energy, 86 (2009) 2071–2078.